



ELSEVIER

FLUID DYNAMICS
RESEARCH

Fluid Dynamics Research 27 (2000) 91–108

Endwall effects in a periodically forced centrifugally unstable flow

J.M. Lopez^{a,*}, F. Marques^b, J. Shen^c

^a*Department of Mathematics, Arizona State University, Tempe AZ 85287-1804, USA*

^b*Departament de Física Aplicada, Universitat Politècnica de Catalunya, Jordi Girona Salgado s/n, Mòdul B4 Campus Nord, 08034 Barcelona, Spain*

^c*Department of Mathematics, Pennsylvania State University, University Park, PA 16802, USA*

Received 20 November 1998; received in revised form 11 October 1999; accepted 5 November 1999

Abstract

Recent experiments of Weisberg et al. (1997. *J. Fluid Mech.* 348, 141–151) have demonstrated that the onset of the centrifugal instability leading to Taylor vortex flow can be delayed by harmonic oscillations of the inner cylinder in the axial direction. Marques and Lopez (1997. *J. Fluid Mech.* 348, 153–175) used Floquet analysis to describe the observed control of the instability over a wide range of frequencies and amplitudes of this oscillation; the dynamics remained axisymmetric and the response to the applied periodic control mechanism was synchronous over an extensive range of parameters. Here we implement an accurate and efficient spectral-projection scheme for solving the fully nonlinear axisymmetric Navier–Stokes equations to examine the effects of endwalls on the flow dynamics and the breaking of space-time symmetries. By varying a single parameter we have detected a route to chaos. As the parameter is increased the system undergoes a quasiperiodic Naimark–Sacker bifurcation, goes through a 1:9 resonance horn (Arnold’s tongue), and then chaos. © 2000 The Japan Society of Fluid Mechanics and Elsevier Science B.V. All rights reserved.

Keywords: Naimark–Sacker bifurcation; Taylor–Couette flow; Route to chaos; Periodic forcing

1. Introduction

1.1. The infinitely long annulus problem

In Hu and Kelly (1995) and Marques and Lopez (1997), the stability of a periodically forced hydrodynamic system was investigated using Floquet theory. The system in question is the flow between two co-axial cylinders of infinite extent, the outer one being stationary and the inner one rotating at some fixed rate (the usual Taylor–Couette flow), and the inner cylinder is also subjected to a harmonic oscillation in the axial direction. A normal mode analysis in the axial direction was

* Corresponding author.

performed in both studies. Hu and Kelly (1995) treated the annulus as open with the pressure being periodic in the axial direction. Marques and Lopez (1997) also considered an enclosed annulus by imposing a zero net mass flux condition via a periodic axial pressure *gradient*. This system has also been investigated experimentally by Weisberg (1996) in an annulus with length-to-gap ratio of 150, with stationary endwalls. In significant regions of parameter space, the Floquet analysis of the open system have large discrepancies with the experiment, but the enclosed system agreed to within experimental uncertainty. Even though the endwalls were modeled as being infinitely far apart (i.e. infinite periodic cylinders), their presence has an order one effect on the dynamics through the imposed zero net axial mass flux. In some parts of parameter space, the onset of instability differed by a factor of two in the critical rotation rate of the inner cylinder between the open and enclosed cases.

The system is governed by a number of nondimensional parameters. Dimensionally, the inner cylinder oscillates in the axial direction with velocity $U \sin \Omega t$ and rotates at constant angular velocity Ω_i . Its radius is r_i and the radius of the outer stationary cylinder is r_o . The annular gap between the cylinders is $d = r_o - r_i$. These parameters are combined to give the following nondimensional governing parameters:

the radius ratio	$e = r_i/r_o$,
the Couette flow Reynolds number	$Re_i = dr_i \Omega_i/\nu$,
the axial Reynolds number	$Re_a = dU/\nu$,
and the nondimensional frequency	$\omega_f = d^2\Omega/\nu$,

where ν is the kinematic viscosity of the fluid. The length and time scales used are the gap, d , and the diffusive time across the gap, d^2/ν , respectively.

The system is governed by the Navier–Stokes equations, which are reduced to a system of ODE by using a Galerkin expansion based on Chebyshev polynomials. The stability analysis of the time-periodic basic state is then reduced to the determination of the growth rates of the solutions of a linear system of the form:

$$F\dot{\mathbf{x}} = H(t)\mathbf{x} = (A + B \sin \omega_f t + C \cos \omega_f t)\mathbf{x}. \quad (1)$$

The entries in the matrices F and H are given in the appendix of Marques and Lopez (1997). H is periodic, of period $T = 2\pi/\omega_f$, where ω_f is the frequency of the axial oscillations of the inner cylinder, and F is time-independent and positive definite. The axial and azimuthal wave numbers of the bifurcating solutions are k and n , respectively.

In the Taylor–Couette flow with axial oscillations of the inner cylinder, the basic state consists of circular Couette flow with a superimposed annular Stokes flow. It is independent of the axial and azimuthal directions, and time-periodic with the period of the forcing; an analytic description of the basic flow is derived in Marques and Lopez (1997). Over an extensive range of parameter space, the primary bifurcation is to an axisymmetric state that is periodic both in the axial direction and in time, with the same temporal period as the forcing (Weisberg et al., 1997; Marques and Lopez, 1997). Small windows of nonaxisymmetric flow in the primary bifurcation have been identified both experimentally (Weisberg, 1997) and numerically (Lopez and Marques, 2000a,b; Marques and Lopez, 2000). However, the synchronous axisymmetric bifurcation is the most common and is the subject of the first nonlinear computational study of this flow presented here.

The Navier–Stokes equations governing this problem are invariant under translations (τ) along and rotations (R) around the common axis of the cylinders. Moreover, the equations are invariant under an additional discrete symmetry (S) involving the time and the axial coordinate; it is a reflection about the plane orthogonal to the axis with a simultaneous time-translation of a half period. Using cylindrical coordinates, they read:

$$(\tau_a \mathbf{u})(r, \theta, z, t) = \mathbf{u}(r, \theta, z + a, t), \quad a \in \mathbb{R} \bmod 2\pi/k, \quad (2)$$

$$(R_\alpha \mathbf{u})(r, \theta, z, t) = \mathbf{u}(r, \theta + \alpha, z, t), \quad \alpha \in \mathbb{R} \bmod 2\pi, \quad (3)$$

$$(S \mathbf{u})(r, \theta, z, t) = (u, v, -w)(r, \theta, -z, t + T/2). \quad (4)$$

The symmetry S satisfies $S^2 = I$, and the symmetry group of our problem is $SO(2) \times O(2)$. The $SO(2)$ factor comes from R_x . The symmetries τ_a and S do not commute, $\tau_a S = S \tau_{-a}$, and give the $O(2)$ factor. The action of $O(2)$ is not the “usual” action because it involves a half-period time translation. The basic state, a limit cycle, is invariant under the full symmetry group of the equations, $SO(2) \times O(2)$. The stability of this basic state is governed by the Floquet multipliers λ of the linear system (1). The basic state becomes unstable when some of these multipliers cross the unit circle through $\lambda = +1$ (synchronous bifurcation), $\lambda = -1$ (subharmonic bifurcation) or a pair of complex conjugate multipliers (Naimark–Sacker bifurcation). The presence of these symmetries has many consequences on the dynamics and the bifurcations this system can experience. In particular, the Z_2 symmetry group generated by S inhibits period doubling ($\lambda = -1$) bifurcations, see Swift and Wiesenfeld (1984), and so only synchronous and Naimark–Sacker bifurcations are allowed for flows with this symmetry. Of course, there may be symmetry breaking bifurcations, and these may be followed by period doublings. Due to the symmetries of the system, the synchronous bifurcation of the basic state is not the generic fold or saddle-node bifurcation, but a pitchfork of revolution. The family of bifurcating solutions is invariant under S and R_x , and its members differ by an axial translation, τ_a (Kuznetsov, 1998; Iooss and Adelmeyer, 1992).

1.2. The finite annulus with stationary endwalls

Benjamin and Mullin (1981) provide compelling theoretical and experimental evidence on the importance of endwall effects in the unforced Taylor–Couette flow, even for very large aspect ratio systems. First, the system goes from having a continuum of possible axial wave numbers to a discrete spectrum. Secondly, the axial dependence of the flow originates in the endwall Ekman layers and exists for all finite Reynolds numbers, Re_i . In the infinite annulus case, the transition to axial variations occurs at a critical Re_i and the bifurcation is a pitchfork of revolution; in the presence of endwalls there is no such bifurcation, and the axial dependence of the flow changes smoothly. Landsberg and Knobloch (1996) provide theoretical arguments based on symmetry considerations, that in closed systems the limit of the aspect ratio *going to* infinity is different to the singular case of the aspect ratio *equal to* infinity. In our system, the presence of endwalls breaks the translational symmetry τ_a and the governing equations have the symmetry group $SO(2) \times Z_2$. Since the Z_2 symmetry is still present, period doubling bifurcations remain inhibited, at least until this symmetry is broken.

The presence of endwalls has implications for the formulation and numerical solution of the problem. The axial direction is no longer periodic; there no longer exists any flow in the finite

system that depends only on (r, t) , all flows are functions of at least (r, z, t) . Not only is a Fourier modal expansion in z prohibited, but one must now solve the governing equations over the whole domain, and the computational cost grows with the aspect ratio.

In the next section we provide a brief description of the nonlinear numerical technique used, and in Section 3 the numerically determined nonlinear dynamics are presented and discussed.

2. Nonlinear numerical scheme

All the previous theoretical results in Marques and Lopez (1997, 2000) discussed above correspond to the idealized case where the length of the annulus is infinite (although the presence of endwalls is accounted for by imposing zero net axial mass flux via the pressure gradient) and only the linear stability of the basic flow was considered. We now study the influence on the nonlinear dynamics due to the finite length of the system in the axisymmetric case.

In order to solve the nonlinear Navier–Stokes equations accurately at low cost, we employ a highly efficient and accurate spectral-projection method in which the time variable is discretized by using a second-order projection scheme (Kan, 1986; Shen, 1996) and the spatial variables are discretized by using a spectral-Galerkin method (Shen, 1994, 1997). We now briefly describe the scheme below and refer to Lopez and Shen (1998) for more details.

The axisymmetric Navier–Stokes equations in cylindrical coordinates can be written in the following vectorial form

$$\mathbf{u}_t - \frac{1}{\text{Re}} \tilde{\Delta} \mathbf{u} + \tilde{\nabla} p + \mathbf{N}(\mathbf{u}) = \mathbf{0} \quad \text{in } \mathcal{D}, \quad \tilde{\nabla} \cdot \mathbf{u} := \frac{1}{r} (ru)_r + w_z = 0 \quad \text{in } \mathcal{D}, \quad (5)$$

where $\mathbf{u} = (u, v, w)^T$, and

$$\tilde{\Delta} = \begin{pmatrix} \tilde{\nabla}^2 - 1/r^2 & 0 & 0 \\ 0 & \tilde{\nabla}^2 - 1/r^2 & 0 \\ 0 & 0 & \tilde{\nabla}^2 \end{pmatrix}, \quad \tilde{\nabla} = \begin{pmatrix} \partial_r \\ 0 \\ \partial_z \end{pmatrix}, \quad \mathbf{N}(\mathbf{u}) = \begin{pmatrix} uu_r + wu_z - v^2/r \\ uv_r + wv_z + uv/r \\ uw_r + ww_z \end{pmatrix}.$$

The domain is $\mathcal{D} = \{(r, z) \mid r \in (r_i, r_0) \text{ and } z \in (-A/2, A/2)\}$, and the velocity \mathbf{u} is subjected to the boundary condition $B(t)\mathbf{u}|_{\partial\mathcal{D}} = 0$, where $B(t)$ is a given operator. Then, the semi-implicit second-order projection scheme for the system of equations (5) is

$$\frac{1}{2\delta t} (3\tilde{\mathbf{u}}^{k+1} - 4\mathbf{u}^k + \mathbf{u}^{k-1}) - \frac{1}{\text{Re}} \tilde{\Delta} \tilde{\mathbf{u}}^{k+1} = -\tilde{\nabla} p^k - 2\mathbf{N}(\mathbf{u}^k) + \mathbf{N}(\mathbf{u}^{k-1}), \quad B(t^{k+1})\tilde{\mathbf{u}}^{k+1}|_{\partial\mathcal{D}} = 0, \quad (6)$$

$$\frac{3}{2\delta t} (\mathbf{u}^{k+1} - \tilde{\mathbf{u}}^{k+1}) + \tilde{\nabla} (p^{k+1} - p^k) = \mathbf{0}, \quad \tilde{\nabla} \cdot \mathbf{u}^{k+1} = 0, \quad (\mathbf{u}^{k+1} - \tilde{\mathbf{u}}^{k+1}) \cdot \mathbf{n}|_{\partial\mathcal{D}} = 0, \quad (7)$$

where δt is the time step, \mathbf{n} is the outward normal at the boundary, and $\tilde{\mathbf{u}}^{k+1} = (\tilde{u}^{k+1}, \tilde{v}^{k+1}, \tilde{w}^{k+1})^T$ and $\mathbf{u}^{k+1} = (u^{k+1}, v^{k+1}, w^{k+1})^T$ are, respectively, the intermediate and final approximations of \mathbf{u} at time

$t^{k+1} = (k + 1) \delta t$. By taking the divergence of the first equation in Eq. (7), we find that system (7) is equivalent (in the space continuous case) to

$$-\tilde{\nabla}^2(p^{k+1} - p^k) = -\frac{3}{2\delta t} \tilde{\nabla} \cdot \tilde{\mathbf{u}}^{k+1},$$

$$\frac{\partial}{\partial \mathbf{n}}(p^{k+1} - p^k)|_{\partial \mathcal{D}} = 0 \tag{8}$$

and

$$\mathbf{u}^{k+1} = \tilde{\mathbf{u}}^{k+1} - \frac{2\delta t}{3} \tilde{\nabla}(p^{k+1} - p^k). \tag{9}$$

Hence, at each time step, we only have to solve a vectorial Helmholtz equation and a scalar Poisson equation both of which can be solved by the fast spectral-Galerkin method (Shen, 1994; Lopez and Shen, 1998).

The flow starts either from rest or as a continuation from a solution with different parameter values, and satisfies the following boundary conditions:

$$u = 0, \quad v = \text{Re}_i, \quad w = \text{Re}_a \sin \omega_f t \quad \text{at } r = r_i,$$

$$u = v = w = 0 \quad \text{at } r = r_0 \text{ and } z = \pm A/2. \tag{10}$$

This flow has discontinuous boundary conditions for v and w , the azimuthal and axial components of velocity, at the corners where the inner cylinder meets the stationary endwalls. Since spectral methods are very sensitive to the smoothness of the solutions, it is crucial to design a sensible treatment for the singular boundary conditions. We emphasize that the singular boundary conditions are usually a mathematical idealization of the physical situation. The singularity can never be realized in experiments nor in numerical computations. Therefore, it is appropriate to use a regularized boundary layer function to approximate the actual physical situation. In fact, the singular boundary conditions at $z = \pm A/2$

$$v = 0 \quad \text{for } r \in (r_i, r_0] \quad \text{and} \quad v = \text{Re}_i \quad \text{at } r = r_i$$

and

$$w = 0 \quad \text{for } r \in (r_i, r_0] \quad \text{and} \quad w = \text{Re}_a \sin \omega_f t \quad \text{at } r = r_i,$$

can be approximated, respectively, by

$$v_\varepsilon(r) = \text{Re}_i \exp\left(-\frac{r - r_i}{\varepsilon}\right), \quad r \in [r_i, r_0] \tag{11}$$

and

$$w_\varepsilon(r) = \text{Re}_a \sin \omega_f t \exp\left(-\frac{r - r_i}{\varepsilon}\right), \quad r \in [r_i, r_0], \tag{12}$$

to within any prescribed accuracy by choosing an appropriate ε . Such an approach has been proved successful in Lopez and Shen (1998) for treating the singular boundary condition for the v component which does not affect the divergence of the axisymmetric velocity field. There, the vortex breakdown flow has been computed to capture the details of the axisymmetric waves/recirculation zones on the axis with high fidelity.

In all our computations, we have used 64×80 modes for all quantities in the spectral-Galerkin formulation. With 64 modes in the radial direction, we were able to use $\varepsilon = 0.005$ in (11–12). Note that further reducing ε without increasing the radial resolution would introduce unwanted oscillations.

For axisymmetric flows in cylindrical geometries, it is typical to present the solutions in terms of the streamfunction ψ , the azimuthal component of vorticity η , and the axial component of the angular momentum $\Gamma = rv$. These are given by

$$(u, v, w) = \left(-\frac{1}{r} \frac{\partial \psi}{\partial z}, \frac{\Gamma}{r}, \frac{1}{r} \frac{\partial \psi}{\partial r} \right),$$

$$\eta = \frac{\partial u}{\partial z} - \frac{\partial w}{\partial r} = -\frac{1}{r} \left(\frac{\partial^2 \psi}{\partial z^2} + \frac{\partial^2 \psi}{\partial r^2} - \frac{1}{r} \frac{\partial \psi}{\partial r} \right).$$

We solve the governing equations using velocity and pressure, and then the azimuthal vorticity η is found by spectral differentiation of u and w , the streamfunction ψ is found by solving the Helmholtz equation with η on the right-hand-side, and Γ by spectral multiplication of rv .

3. Nonlinear dynamics

We have selected to set the gap $e = 0.905$, corresponding to the experiments of Weisberg et al. (1997). The forcing frequency is set to $\omega_f = 30$, well within the region where the Floquet analysis of Lopez and Marques (2000a) and Marques and Lopez (2000) predicts axisymmetric bifurcating solutions. The length to gap ratio is set to $\Lambda = 10$ in this nonlinear study. The dynamics of the flow are investigated as one or the other of the two Reynolds numbers Re_a and Re_i is varied.

3.1. Multiplicity of solutions at fixed Re_i

We begin by considering a path in parameter space with a fixed rotation Reynolds number $Re_i = 200$, and varying the forcing amplitude Re_a . For the infinite case, $\Lambda \rightarrow \infty$, the Floquet analysis predicts a bifurcation to occur at $Re_a \approx 74$ with an axial wave number $k \approx 2.4$, and one would expect to fit four cells with $k = 2.4$ into an $\Lambda = 10$ annulus. Each cell corresponds to an axial wavelength $\lambda = 2\pi/k$, and contains a pair of (counter rotating) Taylor vortices. In a finite annulus, Ekman cells with aspect ratio of about one also form at the endwalls, so that one expects to end up with about three Taylor cells (three pairs of counter rotating Taylor vortices) in the forced system.

For $Re_a > 75$, the system is “stable”. By this we mean that apart from the regions near the endwalls where the Ekman cells are located, the flow in the rest of the annulus is essentially independent of the axial direction. In the $\Lambda \rightarrow \infty$ case, it is clear what is meant by a stable state; the basic state has no axial (z) dependence and instability is characterized by the onset of z -dependence. Fig. 1 shows the contours of the streamfunction ψ (left), azimuthal vorticity η (middle), and axial angular momentum Γ (right) for $Re_a = 100$ over a complete forcing period for $\Lambda = 10$. The flow in the central section of the annulus has the same behavior as the basic state of the $\Lambda \rightarrow \infty$ case, described analytically in Marques and Lopez (1997); it is z -independent and waves of azimuthal vorticity (η) propagate in from the cylinder walls, those from the inner cylinder being more intense than those from the stationary outer cylinder. For finite Λ , the vortex lines are bent near the endwalls and converge to



Fig. 1. Contours of streamfunction ψ (left), azimuthal vorticity η (middle), and axial angular momentum Γ (right) at eight phases over one forcing period $T = 2\pi/\omega_f$ for $Re_i = 200$, $\omega_f = 30$, and $Re_a = 100$. The contour levels are set so that $level_i = C(i/20)^2$, $i = 1 \rightarrow 20$, where $C = \pm 150$ for ψ , $C = \pm 2000$ for η , and $C = 4000$ for Γ ; positive (negative) contours are solid (broken). The computations used 80 axial and 64 radial modes with $\delta t = T/200$.

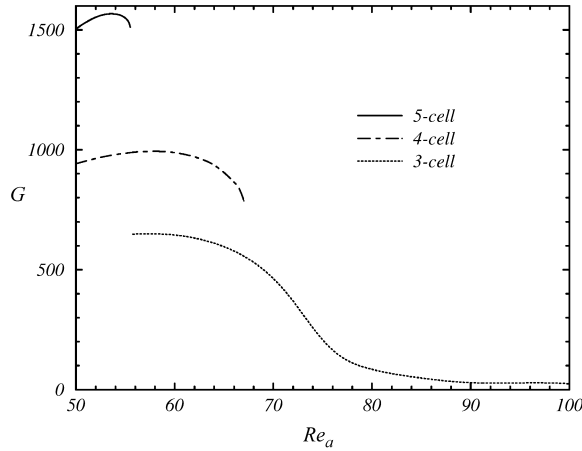


Fig. 2. G versus Re_a , $Re_i = 200$, $\omega_f = 30$, $e = 0.905$, $A = 10$.

the singular corners where the stationary endwalls and the rotating and harmonically oscillating inner cylinder meet, thus producing axial variations in the flow for any finite Re_i or Re_a . This leads to imperfect bifurcations in the finite A cases. An analogous situation for the unforced Taylor–Couette flow in finite annulus has been discussed in detail by Benjamin (1978). As a measure of the flow state, we have selected the following indicator to measure the degree of axial dependence:

$$G = \left(\max_{\text{period}} \|(\partial\Gamma/\partial z)^2\| - \min_{\text{period}} \|(\partial\Gamma/\partial z)^2\| \right), \quad (13)$$

where $\|\cdot\| = \int_{-A/6}^{A/6} \int_0^1 \cdot \, dr \, dz$. Note that in the above definition, the axial dependence near the top and bottom endwalls is excluded in order to capture the main characteristics of the flow in the middle section of the cylinder.

Fig. 2 shows G versus Re_a . Note that there are three distinct branches. The branch labeled 3-cell has roughly three Taylor cells (three pairs of counter rotating vortices) most of the time, branch 4-cell has four, and 5-cell has five. The 3-cell branch shows the typical form of an imperfect bifurcation (it looks like a broken pitchfork), and the unfolding occurs in the vicinity of the perfect bifurcation of the $A \rightarrow \infty$ case, i.e. near $Re_a = 74$. Benjamin and Mullin (1981) have observed in the unforced Taylor–Couette flow with finite aspect ratio a multiplicity of states at the same parameter values, selected by different initial conditions and paths through parameter space. The 3-cell branch loses stability for $Re_a < 55.5$. The 4-cell branch has a turning point at $Re_a \approx 67$, above which it does not exist, and the 5-cell branch has a turning point at $Re_a \approx 55.5$. A full investigation of the possible interconnections between these branches awaits the development of techniques to compute unstable periodic branch solutions for large periodically forced systems.

At zero forcing amplitude, $Re_a = 0$, the Taylor–Couette flow with endwalls is recovered. Fig. 3a shows the contours of the streamfunction ψ (left), azimuthal vorticity η (middle), and axial angular momentum Γ (right) for this case, which is steady. The Taylor vortices are all of square aspect, except for the ones at each end that are modified by the Ekman boundary layer. The Ekman layer is clearly evident from the η contours. The Γ contours, which are the projection of vortex lines onto the meridional plane, illustrate the strong jets emanating from the boundary layer on the inner cylinder

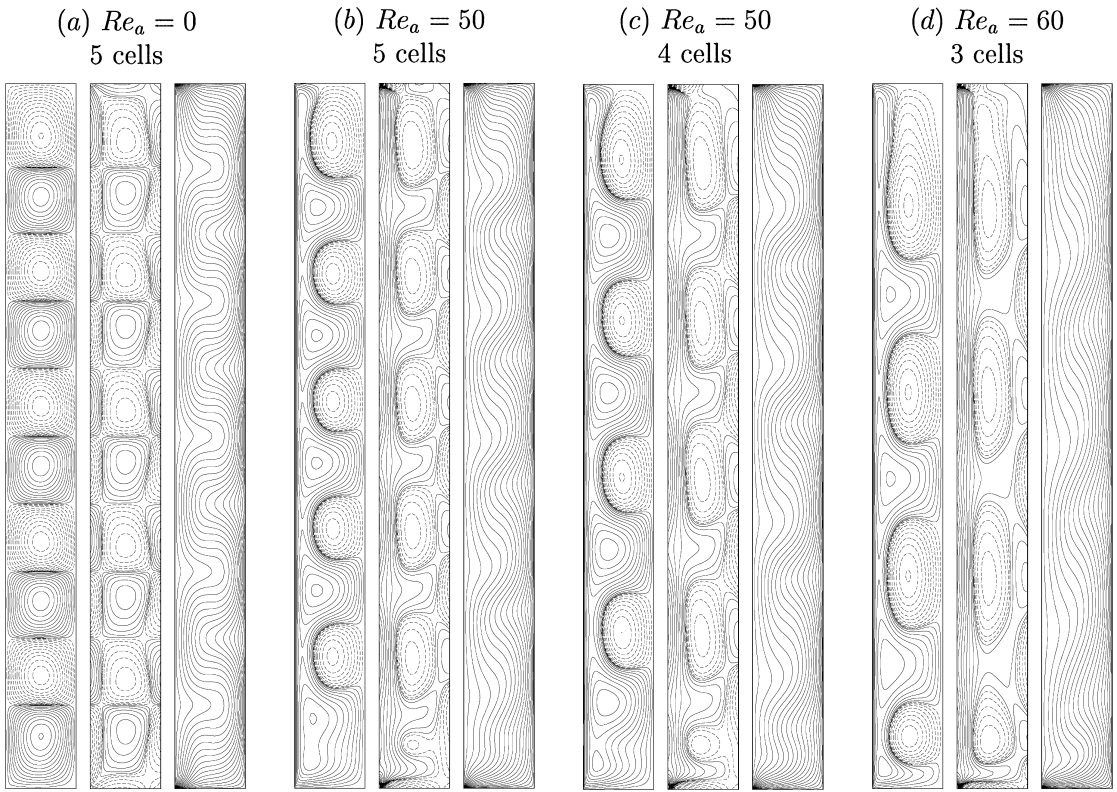


Fig. 3. Contours of streamfunction ψ (left), azimuthal vorticity η (middle), and axial angular momentum Γ (right) at one instant in time, for $Re_i=200$, $\omega_t=30$, and Re_a as indicated. The contour levels are set so that $level_i=C(i/20)^2$, $i=1 \rightarrow 20$, where $C = \pm 100$ for ψ , $C = \pm 1000$ for η , and $C = 2000$ for Γ ; positive (negative) contours are solid (broken). The computations used 80 axial and 64 radial modes with $\delta t = T/200$.

as well as the weaker jets from outer cylinder boundary layer. These features of the flow agree with the computations in an infinite annulus of Fazel and Booz (1984), apart from the effects of the endwalls. The Taylor vortices are paired up, about the jet from the inner cylinder. This solution corresponds to the primary branch of solutions found by Benjamin and Mullin (1981) in finite annuli. Benjamin and Mullin (1981, 1982) also found a multiplicity of solutions in these finite annuli, but the branches with an even number of Taylor vortices, which paired up about the outgoing jet, are more robust and appear at lower Re_i than the so-called anomalous modes with an odd number of Taylor vortices.

We have also observed a multiplicity of solutions in the forced system. All of these correspond to the robust states with an even number of vortices. Figs. 3b and c show two such states for the same parameter values (arrived at from different initial conditions), where in one case the Taylor vortices have paired up to form five cells (this branch continues to the $Re_a=0$ state in Fig. 3a) and the other case has four cells. Fig. 3d is of a 3-cell solution at $Re_a = 60$. These figures are of instantaneous quantities, at about the same phase of the forcing. At this phase, the structures are most similar to the structures in the unforced system shown in Fig. 3a. When $Re_a \neq 0$, the axial oscillations of the

inner cylinder generates waves of azimuthal vorticity η in the Stokes layer close to the inner wall, that penetrate into the bulk of the fluid, reinforcing the Taylor vortices with an η of the same sign as the wave, and damping the Taylor vortices with an opposite sign of η . This is the fundamental physical mechanism in delaying the transition from the basic flow to the periodic Taylor vortices, as explained in detail in Marques and Lopez (1997). During half a period of the axial oscillation, the reinforced Taylor vortices grow at the expense of the damped vortices, almost dominating a cell; during the other half period the situation is reversed. During the time evolution, the outgoing jet moves up and down, oscillating in the axial direction; this behavior can be observed in Fig. 4. We believe this strong interaction between vortices reinforces their pairing around the outgoing jet, and makes it more difficult (if not impossible) to find anomalous modes.

3.2. A route to chaos with increasing Re_i

All the solution branches depicted in Fig. 2 are synchronous with the forcing and preserve the S symmetry (half-period time translation plus a reflection $z \rightarrow -z$). We now consider a different path through parameter space. All the parameters are kept as in the previous parameter study, except that now we fix $Re_a = 80$ and vary Re_i from 200 up.

The function $G(t)$ introduced in Eq. (13) is a quadratic measure of the z -dependence of the flow. Due to the S symmetry, G has a period half of the forcing, and a corresponding doubled frequency (see Knobloch et al., 1986 for a flow problem with the same symmetry S). In order to avoid this apparent frequency doubling, we use the time series of the radial velocity u and angular momentum Γ at a specific point Q of the domain. A convenient Gauss–Lobato point ($r = r_i + 0.573$, $z = 0.969$) was selected in order to avoid symmetrical points in the domain. As we are dealing with bifurcations of a limit cycle, the corresponding Poincaré map is particularly useful. Since the forcing frequency is known and fixed, we have a global Poincaré map

$$P: \mathbf{u}(r, \theta, z, t) \rightarrow \mathbf{u}(r, \theta, z, t + T).$$

The introduction of this map simplifies the description of the dynamics; the periodic solutions, synchronous with the forcing, are fixed points of P . An invariant 2-torus becomes a closed invariant curve of P .

At $Re_i = 280$, the flow corresponds to the 3-cell branch, and is synchronous with the forcing. The projection of the trajectory in the phase plane $(u, \Gamma)_Q$ for $Re_i = 280$, shown in Fig. 5a, as well as the corresponding power spectral density (PSD) of $\Gamma_Q(t)$ in Fig. 6a, indicate the limit cycle behavior.

By $Re_i = 281$, a Naimark–Sacker bifurcation has occurred. The phase portrait depicted in Fig. 5b suggests that the limit cycle behavior observed at the lower Re_i has given way to a 2-torus. The corresponding Poincaré map (Fig. 7a) clearly shows the presence of an invariant circle. Note that the trajectory on the circle is not uniform, but shows the typical bottleneck behavior associated with a nearby saddle-node bifurcation. The PSD of $\Gamma_Q(t)$ in Fig. 6b contains the forcing frequency and its harmonics, a relatively strong second frequency, $\omega_s \approx 3.1$, and a sequence of linear combinations between ω_s and ω_f . The weak signal at $\omega < \omega_s$ is due to ω_s and ω_f being incommensurate. The two frequencies ω_s and ω_f are close to a 1:9 resonance, and hence the ‘clean’ PSD and the bottleneck behavior.

Increasing Re_i to 282, the solution branch undergoes a saddle-node bifurcation as it enters a 1:9 resonance horn. This is evident from the phase portrait, PSD, and Poincaré map, depicted in

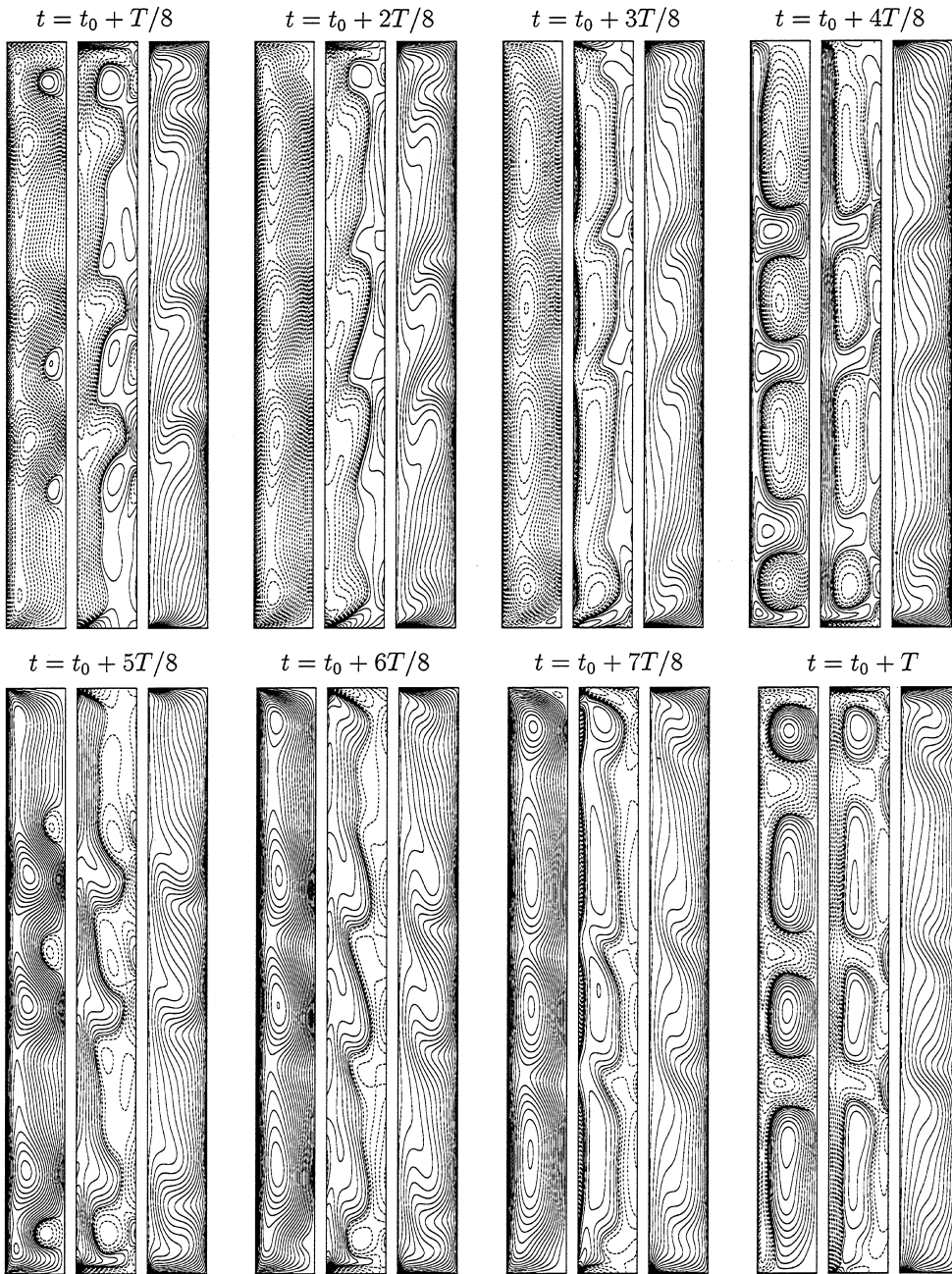


Fig. 4. Contours of streamfunction ψ (left), azimuthal vorticity η (middle), and axial angular momentum Γ (right) at eight phases over one forcing period $T = 2\pi/\omega_f$ for $Re_i = 280$, $\omega_f = 30$, and $Re_a = 80$. The contour levels are set so that $level_i = C(i/20)^2$, $i = 1 \rightarrow 20$, where $C = \pm 150$ for ψ , $C = \pm 2000$ for η , and $C = 4000$ for Γ ; positive (negative) contours are solid (broken). The computations used 80 axial and 64 radial modes with $\delta t = T/200$.

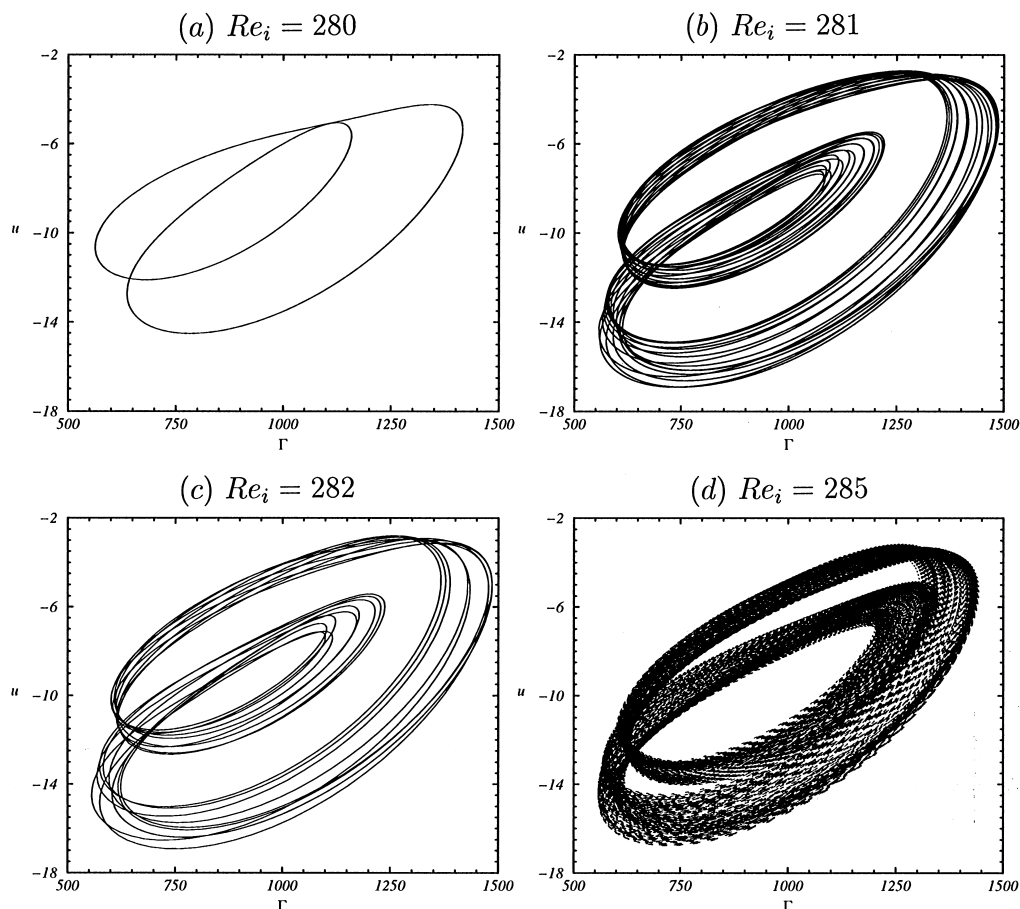


Fig. 5. Projections of phase portraits onto the $(u, \Gamma)_Q$ plane for $Re_a = 80$, $\omega_f = 30$, $e = 0.905$, $A = 10$, and Re_i as indicated.

Figs. 5c, 6c, and 7b. In the Poincaré map, we have indicated the order in which the iterates of the map appear. The ordering is a strong indication that the locking is 1:9, rather than $n:9$ with $n > 1$.

Increasing Re_i beyond 282, the solution leaves the 1:9 resonance horn, and by $Re_i = 285$ behavior characteristic of chaos is observed. The phase portrait (Fig. 5d) and the PSD (Fig. 6d) on their own are not sufficient for such a conclusion. However, the Poincaré map shows clear evidence of the breakup of the 2-torus (Fig. 7c).

The onset of a Naimark–Sacker bifurcation from a limit cycle to a 2-torus just described above has occurred in an axisymmetric system. It should be noted that Naimark–Sacker bifurcations detected in the stability analysis of the basic state in the $A \rightarrow \infty$ system have always been associated with the simultaneous breaking of the S and the azimuthal symmetry (Lopez and Marques, 2000b). The windows in parameter space that include Naimark–Sacker bifurcations in the infinite system have lower forcing frequencies than that considered here ($\omega_f = 30$). Typically these are between 7 and 12 for $Re_a = 80$ (Marques and Lopez, 2000). At the forcing frequency considered here, $\omega_f = 30$, the first bifurcation in the *infinite* system is axisymmetric and synchronous. It is a pitchfork of revolution, the

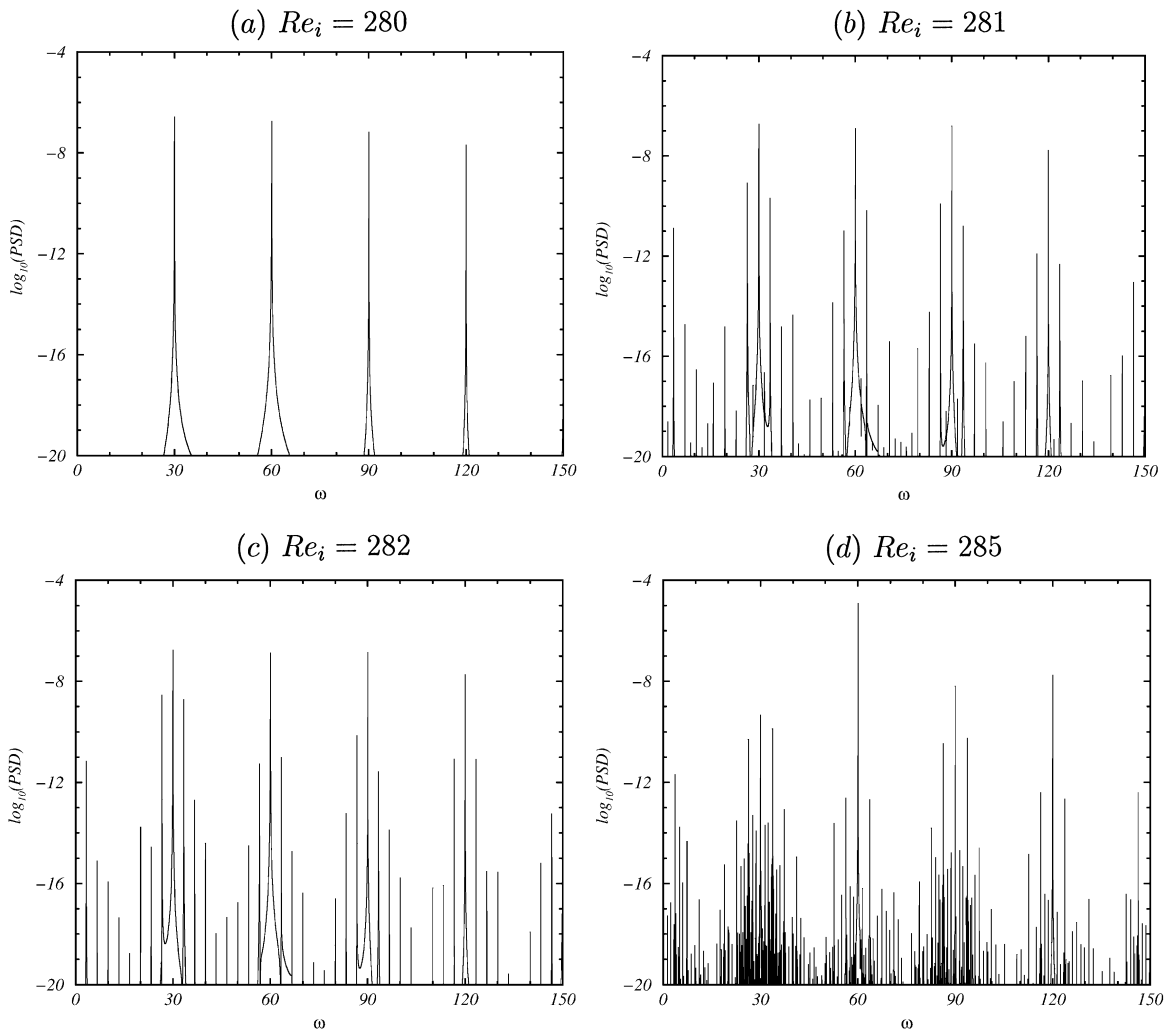


Fig. 6. Power spectral density of Γ_Q for $Re_a = 80$, $\omega_f = 30$, $e = 0.905$, $A = 10$, and Re_i as indicated. The PSD were taken from a time series covering approximately $10,500T$, i.e. 2^{21} points with $\delta t = T/200$, after allowing transients to die out over a similar length of time.

bifurcating solutions are invariant under S and R_z , and differ by an axial translation τ_a . Subsequent secondary bifurcations may break the S symmetry, or the azimuthal symmetries R_z , or both. However, they have not yet been investigated in the infinite annulus case. In the finite system with endwalls we have a smooth transition from the basic flow without axial dependence in the bulk for low Re_i , to the 3-cell flow when Re_i is increased. This smooth transition (imperfect bifurcation) replaces the first axisymmetric bifurcation in the infinite system, and in both cases the emerging solution keeps the symmetry group $SO(2) \times Z_2$ generated by R_z and S . The first axisymmetric bifurcation we have found in the *finite* system is a quasiperiodic Naimark–Sacker, and as Re_i increases the system goes through a 1:9 soft resonance horn and then into a chaotic regime. The breaking of the S symmetry

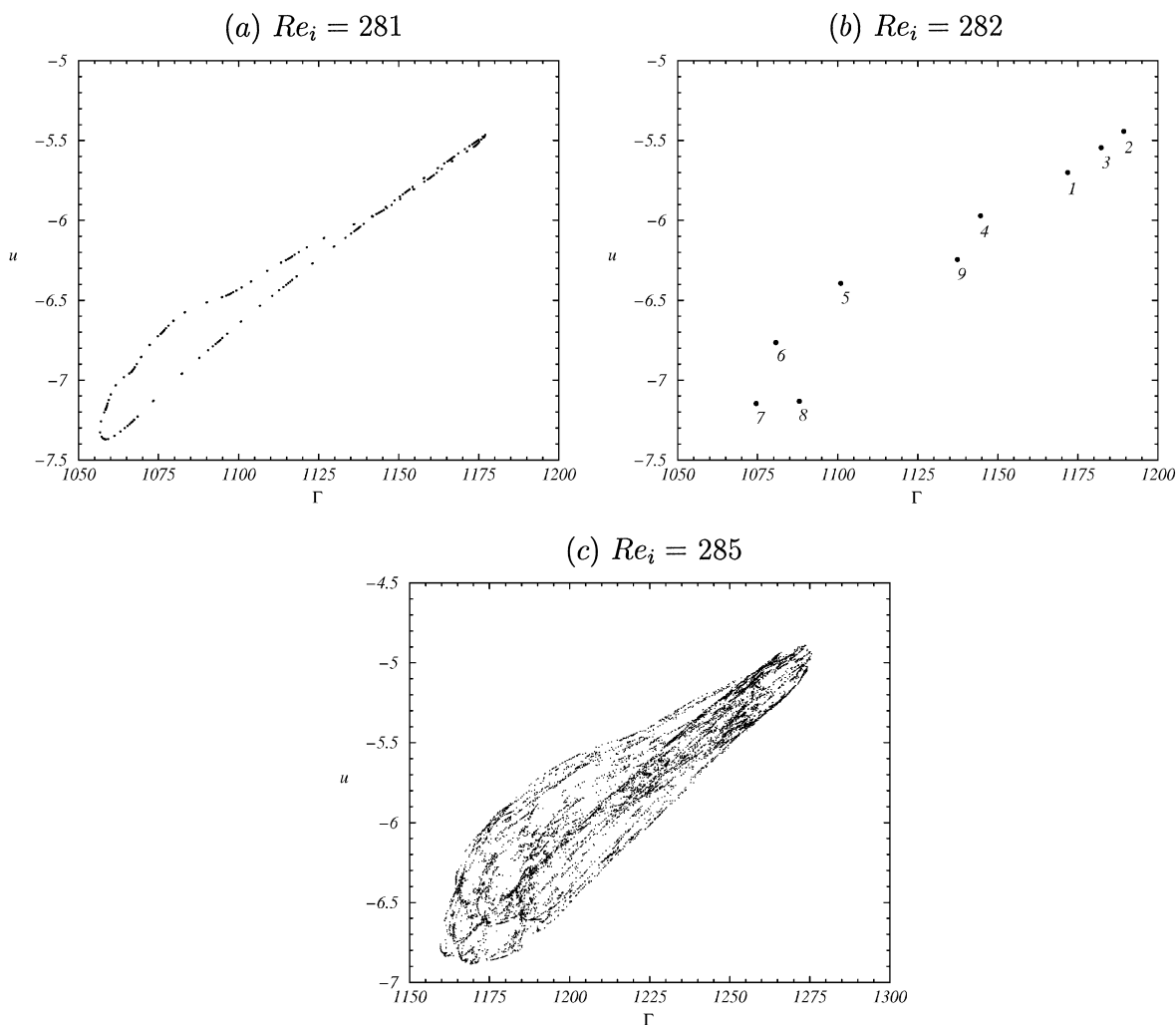


Fig. 7. Poincaré maps of the phase trajectories shown in Fig. 5 for $Re_a = 80$, $\omega_f = 30$, $e = 0.905$, $A = 10$, and Re_i as indicated. For the locked case of $Re_i = 282$, the order in which the trajectory passes through the Poincaré map is indicated.

in this bifurcation, seems to be due to the nonlinear coupling between the Ekman vortices on the endwalls and the Taylor vortices in the interior.

The evolution of the solution for $Re_i = 280$ and $Re_a = 80$ over one complete period of the forcing $T = 2\pi/\omega_f$, shown in Fig. 4, corresponds to the limit cycle in Fig. 5a. It is clear that the discrete symmetry S is preserved in this highly nonlinear flow; the four snapshots in the first half period are the same as the next four after they are reflected in the cylinder half-height and $\psi \rightarrow -\psi$ and $\eta \rightarrow -\eta$. The Taylor vortices at $Re_i = 280$ and $Re_a = 80$ are no longer apparent; they are only seen for a very short part of the period (about $t + T/2$ and $t + T$ in the Fig. 4). Over the majority of the period, the flow is dominated by cellular structures with azimuthal vorticity of the same sign as that of the inner boundary layer. The only coherent structures that are common to the unforced

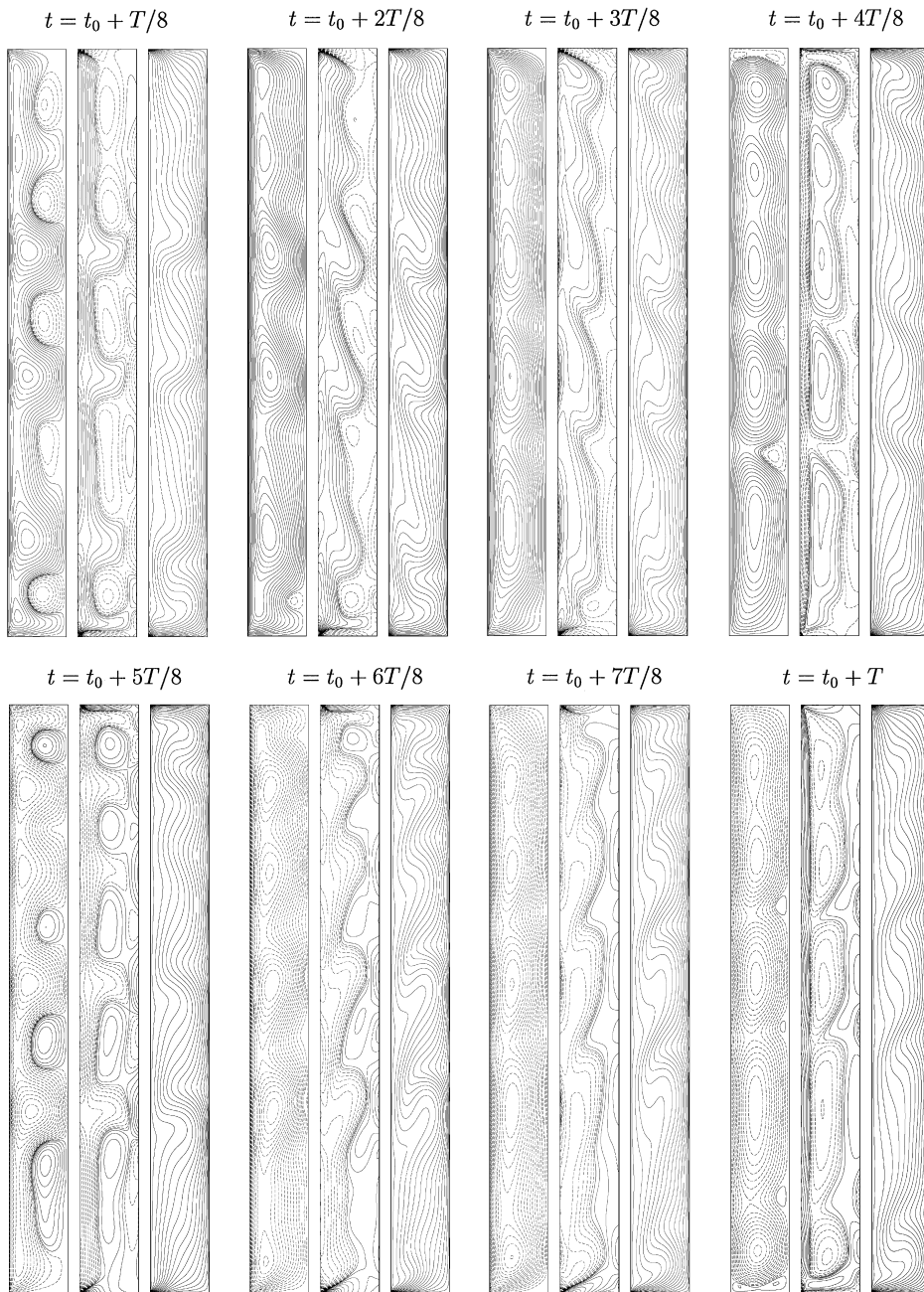


Fig. 8. Contours of streamfunction ψ (left), azimuthal vorticity η (middle), and axial angular momentum Γ (right) at eight phases over one forcing period $T = 2\pi/\omega_f$ for $Re_i = 282$, $\omega_f = 30$, and $Re_a = 80$. The contour levels are set so that $level_i = C(i/20)^2$, $i = 1 \rightarrow 20$, where $C = \pm 150$ for ψ , $C = \pm 2000$ for η , and $C = 4000$ for Γ ; positive (negative) contours are solid (broken). The computations used 80 axial and 64 radial modes with $\delta t = T/200$.

Taylor–Couette flow and are preserved over the entire period are the jets emanating from the inner cylinder. The flow is highly distorted, compared to the unforced and the weakly forced systems in Fig. 3, and a distinct axial wavelength is no longer apparent. Nevertheless, the solution depicted in Fig. 4 belongs to the 3-cell family, and at all times three strong jets are evident.

In increasing Re_i from 280 to 281, the system undergoes an S-symmetry breaking Naimark–Sacker bifurcation. Fig. 8 shows the evolution of the solution for $Re_i = 282$ and $Re_a = 80$ over one complete period of the forcing $T = 2\pi/\omega_f$, corresponding to the frequency locked state in Figs. 5c, 6c, and 7b. The symmetry breaking is evident in all of these figures. In the solution contour plots, the symmetry breaking is most pronounced in the regions near the endwalls; the presence of a second frequency in the PSD, and the 2-torus structure in the phase portrait and Poincaré map are also clearly evident.

In the infinite annulus case, Naimark–Sacker bifurcations have only been found breaking the azimuthal and S symmetries simultaneously, and at much smaller forcing frequencies. A novel effect of the endwalls in the finite case is that the S symmetry is broken axisymmetrically. In the absence of the axial forcing, the jets emanate from the inner cylinder at fixed specific locations. The axial oscillations tend to drag the jets axially causing them to interact with the Ekman layers on the endwalls. When the intensity of the jets is sufficiently large (for larger Re_i), this interaction with the endwalls is likely to be the physical mechanism that breaks the S symmetry.

4. Summary

We have presented a numerical study of a periodically forced centrifugally unstable flow, well into the nonlinear regime. For the physically realistic case of finite length annulus, the endwalls and the finite aspect ratio of the annulus are dynamically important. These nonlinear effects are investigated with a very efficient and accurate spectral-projection method for solving the fully nonlinear axisymmetric Navier–Stokes equations. We have focused our attention on the axisymmetric states, guided by the results of the fully three-dimensional Floquet analysis, and considered two scenarios: either varying the forcing amplitude Re_a or the Couette flow Reynolds number Re_i , while keeping other parameters fixed.

At a set value of $Re_i = 200$ and reducing Re_a from 100 to 50, the nonlinear response of the system was synchronous with the forcing frequency. The flow underwent a smooth transition from a flow with essentially no axial variation, other than near the endwalls, for $Re_a \gtrsim 80$, to a state with Taylor cells for $Re_a \lesssim 70$. As Re_a was further reduced, additional solution branches, all synchronous with the forcing, were encountered. The existence of multiple flow states with differing length scales is typical of pattern forming systems in enclosed regions. The multiplicity of states is consistent with two previously known limits: (i) when the forcing amplitude goes to zero, $Re_a \rightarrow 0$, the 5-cell flow corresponding to the unforced Taylor vortex flow is recovered; and (ii) when $Re_a \rightarrow Re_a^{\text{crit}}$, the critical Re_a for the infinite system, the predicted 3-cell flow is also recovered.

When Re_a was fixed and Re_i increased, we encountered a Naimark–Sacker bifurcation breaking the space-time discrete symmetry S and leading to flow on a 2-torus. The solution subsequently followed a Ruelle–Takens route to chaos, in this case through a 1 : 9 resonance horn. The numerical results suggest that this bifurcation sequence is physically due to the coupling between the Taylor–Stokes vortices and the endwall Ekman vortices.

In this paper, only axisymmetric computations have been made, because the primary bifurcation in the infinite system is axisymmetric in the range of amplitude and frequency of the forcing considered, as well as for obvious computational reasons. It is still possible that the finite system undergoes a nonaxisymmetric bifurcation before the Naimark–Sacker bifurcation. This could be tested experimentally or numerically, using 3D codes or performing a linear stability analysis of the axisymmetric 3-cells flow. The associated computational costs are very large, but these are necessary tasks to be addressed in the near future. As an indication of the computational cost involved in the present axisymmetric computations, the use of 64×80 spectral modes with $\delta t = T/200$ on a single MIPS R10000 CPU takes approximately 26 s per period T , and typical runs with one set of parameter values cover 20,000 T .

Acknowledgements

This work was supported by NSF grants DMS-9706951 and INT-9732637, and SEEUID grants PB97-0685 and PR1999-0272.

References

- Benjamin, T.B., 1978. Bifurcation phenomena in steady flows of a viscous fluid. *Proc. Roy. Soc. London A* 359, 1–26.
- Benjamin, T.B., Mullin, T., 1981. Anomalous modes in the Taylor experiment. *Proc. Roy. Soc. London A* 377, 221–249.
- Benjamin, T.B., Mullin, T., 1982. Notes on the multiplicity of flows in the Taylor experiment. *J. Fluid Mech.* 121, 219–230.
- Fazel, H., Booz, O., 1984. Numerical investigation of supercritical Taylor vortex flow for a wide gap. *J. Fluid Mech.* 138, 21–52.
- Hu, H.C., Kelly, R.E., 1995. Effect of a time-periodic axial shear flow upon the onset of Taylor vortices. *Phys. Rev. E* 51, 3242–3251.
- Iooss, G., Adelmeyer, M., 1992. *Topics in Bifurcation Theory and Applications*. World Scientific, Singapore.
- Kan, J.V., 1986. A second-order accurate pressure-correction scheme for viscous incompressible flow. *SIAM J. Sci. Statist. Comput.* 7, 870–891.
- Knobloch, E., Moore, D., Toomre, J., Weiss, N., 1986. Transitions to chaos in two-dimensional double-diffusive convection. *J. Fluid Mech.* 166, 409–448.
- Kuznetsov, Y.A., 1998. *Elements of Applied Bifurcation Theory*, 2nd Edition. Springer, Berlin.
- Landsberg, A.S., Knobloch, E., 1996. Oscillatory bifurcation with broken translation symmetry. *Phys. Rev. E* 53, 3579–3600.
- Lopez, J.M., Marques, F., 2000a. Determining the self-rotation number following a Naimark–Sacker bifurcation in the periodically forced Taylor-Couette flow. *Z. Angew. Math. Phys.*, to appear.
- Lopez, J.M., Marques, F., 2000b. Quasiperiodic response to parametric excitations. In: Tuckerman, L., Doedel, E. (Eds.), *Numerical Methods for Bifurcation Problems and Large Scale Dynamical Systems*, Springer-Verlag IMA Volumes in Mathematics and its Applications, Vol. 119. pp. 209–228.
- Lopez, J.M., Shen, J., 1998. An efficient spectral-projection method for the Navier–Stokes equations in cylindrical geometries I. Axisymmetric cases. *J. Comput. Phys.* 139, 308–326.
- Marques, F., Lopez, J.M., 1997. Taylor-Couette flow with axial oscillations of the inner cylinder: Floquet analysis of the basic flow. *J. Fluid Mech.* 348, 153–175.
- Marques, F., Lopez, J.M., 2000. Spatial and temporal resonances in a periodically forced extended system. *Physica D*, 136, 340–352.
- Shen, J., 1994. Efficient spectral-Galerkin method I. direct solvers for second- and fourth-order equations by using legendre polynomials. *SIAM J. Sci. Comput.* 15, 1489–1505.

- Shen, J., 1996. On error estimates of projection methods for the Navier-Stokes equations: Second-order schemes. *Math. Comput.* 65, 1039–1065.
- Shen, J., 1997. Efficient spectral-Galerkin methods III. Polar and cylindrical geometries. *SIAM J. Sci. Comput.* 18, 1583–1604.
- Swift, J.W., Wiesenfeld, K., 1984. Suppression of period doubling in symmetric systems. *Phys. Rev. Lett.* 52, 705–708.
- Weisberg, A.Y., 1996. Control of transition in Taylor-Couette flow with axial motion of the inner cylinder. Ph.D. Thesis, Princeton University.
- Weisberg, A.Y., Kevrekidis, I.G., Smits, A.J., 1997. Delaying transition in Taylor-Couette flow with axial motion of the inner cylinder. *J. Fluid Mech.* 348, 141–151.